

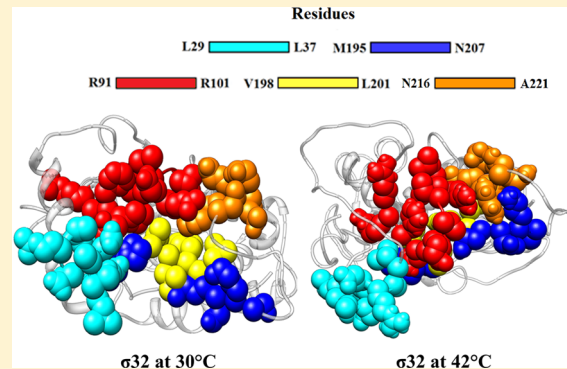
Conformational Adaptation in the *E. coli* Sigma 32 Protein in Response to Heat Shock

Abhijit Chakraborty,[†] Srijata Mukherjee,[†] Ruchira Chattopadhyay, Siddhartha Roy,* and Saikat Chakrabarti*

Division of Structural Biology and Bioinformatics, CSIR-Indian Institute of Chemical Biology, 4, Raja S.C. Mullick Road, Kolkata 700 032, India

Supporting Information

ABSTRACT: *E. coli*, like other organisms, responds to heat shock by rapidly up-regulating several proteins, including chaperones. The heat-shock sigma factor, sigma 32 (σ^{32}), a transcription factor, plays a pivotal role in this response. The level of σ^{32} is normally kept low through a DnaK/J mediated degradation. Elevated temperature rapidly increases the σ^{32} level and initiates a heat-shock response. A plausible way for the up-regulation of free σ^{32} levels would be to destabilize the σ^{32} :DnaK:DnaJ complex initiated via a conformational change in σ^{32} structure at elevated temperatures. In this study, we have modeled the *E. coli* σ^{32} structure by homology modeling and conducted extensive molecular dynamics (MD) simulations at non-heat-shock (30 °C) and heat-shock (42 °C) temperatures. Substantial structural rearrangements at 42 °C were observed around the N-terminus (residues 11–60, which cover the DnaJ binding region) and the region spanning residues 190–210 (covering the DnaK binding site, residues 198–201). At 42 °C, a large amount of helix melting and structural destabilization was observed around residues 11–60, while regions 91–101 and 216–221 of σ^{32} undergo conformational change, leading to formation of a lid-like structure over region 198–VLYL-201 resulting in reduced accessibility of the DnaK binding sites. These temperature induced melting and fluctuations observed around the DnaJ and/or DnaK binding regions suggest reduction of DnaK/DnaJ affinity for σ^{32} at 42 °C, which is further supported by our molecular docking analysis. Emission maxima of environment sensitive fluorescence probes inserted at several cysteine mutants of σ^{32} protein at 30 and 42 °C are also supportive of the structural changes observed in the molecular dynamics study.



INTRODUCTION

Organisms respond to elevation of temperature by rapidly up-regulating proteins that counteract the effect of high temperatures, e.g., chaperones. Response to elevated temperatures, i.e., the heat-shock response, is universal in all organisms.¹ The heat-shock response has been studied in many organisms over the last several decades, but many aspects are still unclear. Heat-shock response in bacteria is generally believed to be initiated by binding of heat-shock sigma factors to the core RNA polymerase, forming the respective holoenzymes.² Bacteria, in general, have several sigma factors, each capable of recognizing a different class of promoter.³ Sigma factors are in equilibrium between the free state and bound to several partner proteins that include anti-sigma factors and the core RNA polymerase.⁴ The holoenzyme level specific to a sigma factor is thought to be directly related to the concentration of the free sigma factor. Promoter class-specific genetic programs of bacteria are often initiated by increased binding of specific sigma factors to the core RNA polymerase, forming the respective RNA polymerase holoenzyme.⁵ The concentrations of respective holoenzymes are believed to be the crucial factor in regulating promoter class-specific gene expression. Thus, regulation of the level of

sigma factors is one of the important mechanisms of regulating class-specific gene expression programs.

Heat-shock response in *E. coli* is dependent upon gene expression from sigma 32 (σ^{32})-specific promoters. Under normal conditions, σ^{32} is complexed with DnaK/DnaJ proteins leading to the degradation of σ^{32} , predominantly by the membrane bound AAA-protease FtsH.^{6,7} Upon elevation of temperature, cellular concentration of σ^{32} is rapidly up-regulated. This in turn leads to elevated concentration of σ^{32} . RNA polymerase holoenzyme complex and consequently transcription of several genes are responsible for the heat-shock response.⁸ The up-regulation of the σ^{32} level probably happens by more than one mechanism, out of which the dissociation of the σ^{32} :DnaK:DnaJ complex is probably the most important.^{7,9} Destabilization of the σ^{32} :DnaK:DnaJ complex at elevated temperatures leads to up-regulation of the σ^{32} level, consequent formation of the σ^{32} :core RNA

Received: February 5, 2014

Revised: April 8, 2014

Published: April 25, 2014



polymerase complex, and initiation of transcription of heat-shock genes.

One proposed mechanism of destabilization of the σ^{32} :DnaK:DnaJ complex is through competition with unfolded proteins at elevated temperatures.¹⁰ In previous studies, reduction of helix content and enhancement of amide hydrogen exchange was seen in σ^{32} upon shift of temperature to 42 °C,^{11,12} suggesting a temperature dependent conformational change. In this article, the effect of temperature on the structure of σ^{32} was shown using exhaustive molecular dynamics and fluorescence spectroscopy studies. Further, via extensive protein–protein docking analysis, we explored the rationality of a plausible mechanism of disruption of σ^{32} :DnaK:DnaJ complex upon elevation of temperature arising due to a conformational change that occurs in the σ^{32} structure. On the basis of a successful combination of computational and experimental techniques, we demonstrated considerable structural rearrangements around the DnaK and DnaJ binding sites at a higher temperature (42 °C), probably leading to compromised σ^{32} :DnaK:DnaJ complex formation and/or probable disruption of the complex.

MATERIALS AND METHODS

Materials. All reagents and materials used in this study were of analytical grade and purchased from standard companies. Details about materials and methods are provided in jp501272n_si_001.pdf in the Supporting Information.

Site Directed Mutagenesis, Protein Purification, and Chemical Modification. The mutant genes were constructed by the overlap extension procedure using the high-fidelity *Pfu* DNA polymerase as described before.¹³ Details about the plasmid generation, protein purification, and IAEDANS labeling are provided in jp501272n_si_001.pdf in the Supporting Information.

Fluorescence Studies. All fluorescence spectra were measured in a Hitachi F 3010 spectrofluorimeter having a facility for spectra addition and subtraction. Fluorescence anisotropy measurements were performed using a Hitachi polarizer accessory. Please refer to jp501272n_si_001.pdf in the Supporting Information for an elaborate description about the fluorescence anisotropy and temperature dependent fluorescence emission analysis.

Energy Transfer from 5-OH Trp Labeled DnaK to AEDANS- σ^{32} . Ten μM IAEDANS labeled sigma 32 and 10 μM 5-OH tryptophan incorporated DnaK were prepared separately and mixed by adding weighed amounts. The mixture was allowed to incubate for half an hour, and then the spectra were taken. Further details about the energy transfer efficiency can be found in jp501272n_si_001.pdf in the Supporting Information.

Fold Recognition, Template Selection, and Homology Modeling. Primary sequences corresponding to σ^{32} were obtained from UniProt¹⁴ with identifier P0AGB3 and subjected to secondary structure prediction and fold recognition by HHpred,¹⁵ PHYRE,¹⁶ and PSI-PRED¹⁷ servers. Three-dimensional (3D) coordinates of the best template structure, sigma factor σ^{28} of *Aquifex aeolicus* (PDB: 1RP3 chain A, closed state), were used to model the closed state of σ^{32} as opposed to the RNA polymerase bound open state. Modeler v9.9¹⁸ was invoked to generate the tertiary coordinates for the monomeric subunit of σ^{32} . The DnaJ (Uniprot ID: P08622) model was also generated using the Modeler v9.9¹⁸ program. At the first step, a multitemplate based model was generated using PDB IDs

1BQ0¹⁹ (*E. coli* DnaJ) and 4J80²⁰ (*Thermus thermophilus* DnaJ) and a refined DnaJ model of *E. coli* template from the SWISS-MODEL Repository,^{21,22} followed by a restrained modeling using 1EXK²³ (*E. coli* DnaJ). The DnaJ structure was then energy minimized through a steepest-descent and conjugate gradient procedure²⁴ and was further used for the docking procedure. The relevant details regarding the 3D model validation and stereochemical quality are provided in Table S2 and Figure S1 of jp501272n_si_002.pdf in the Supporting Information.

Molecular Dynamics Simulation Protocol. The monomer coordinates of the *E. coli* sigma factor σ^{32} homology model were taken as the starting structure for initiating molecular dynamics (MD) simulations (see also Table S1 in jp501272n_si_001.pdf in the Supporting Information) at 30 °C temperature. All simulations were performed using GROMACS v4.5.3 and v4.6.1.²⁵ The united atom force field GROMOS96 53a6²⁶ was used to describe protein, water, and ions. The elevated temperature simulation was performed at $T = 315$ K (42 °C) to assess the heat-shock conditions in σ^{32} , keeping the other simulation parameters the same. A total production run of 800 ns (300 ns at 30 °C and 500 ns at 42 °C) was done on five HP Proliant 160 G6 machines, each having six Intel Zeon X5675 (3.07 GHz processors) in HPC clusters. All other details relevant to the molecular dynamics simulation are provided in Table S1 of jp501272n_si_001.pdf in the Supporting Information.

MD Trajectory Analysis. The emergent trajectories were analyzed by employing the built-in tools of GROMACS v4.5.3 and v4.6.1. The calculations of *root-mean-square deviation* (RMSD) and *root-mean-square fluctuation* (RMSF) were made with respect to the starting structure. The time dependent change of the virtual dihedral (τ_v) comprising C^α atoms of residues 37-81-107-971 and the distribution of angle (θ) and dihedral (τ_d) formed between C^α atoms of residues 37-81-107 and 37-81-107-97, respectively, were calculated. MUSTANG v3.2.1²⁷ was used for structural superimposition. VMD v1.8.7²⁸ and CHIMERA v1.5.3²⁹ were used for visualization. All molecular graphics images were created using CHIMERA v1.5.3.²⁹

Protein–Protein Docking Analysis. Docking of the DnaK structure (PDB ID: 4JN4)³⁰ and the DnaJ 3D model onto the equilibrated structure of σ^{32} was done using PatchDock³¹ followed by an extensive refinement by the FireDock³² program. Best docked poses were selected from the most populated docked solution cluster followed by critical manual inspection satisfying favorable interactions between the interacting motifs of the two proteins. Geometrical score and free energy for binding [ΔG (kcal/mol)] values were further used to compare the docking poses obtained with σ^{32} structures at 30 and 42 °C temperatures, respectively. Geometrical score and free energy for binding were calculated using the PatchDock³¹ and PDBePISA (v1.48)³³ programs, respectively.

RESULTS AND DISCUSSION

Modeling of σ^{32} Structure in the Closed State. Full length free sigma factors have not been crystallized yet. However, a number of anti-sigma factor bound cocrystal structures are known.^{34,35} Previous studies have indicated that free sigma factors are largely observed in a compact form resembling the anti-sigma factor bound state, which we term the closed state.³⁴ Thus, we built a homology model of σ^{32} based on the anti-sigma factor bound σ^{28} crystal structure

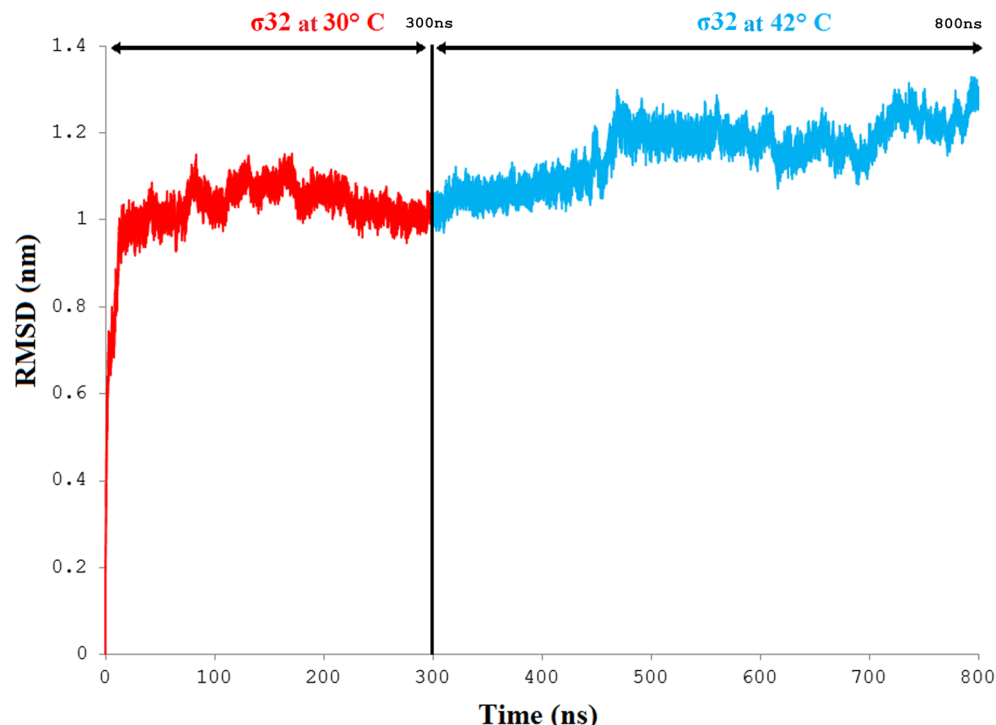


Figure 1. Root-mean-square deviation (RMSD) plot showing the overall fold conservation of σ^{32} . RMSD was calculated with respect to the starting structure, and the C $^{\alpha}$ to C $^{\alpha}$ atom fitting was done. The emergent trajectories obtained at simulated temperatures of 30 °C (red) and 42 °C (blue) show subtle deviation from starting conformations. The ribbon representations of superimposed structures saved at time intervals of $t = 0$ (dark gray), 300 (red), and 800 ns (blue) are presented on top. The RMSD values are reported for the compared structures from σ^{32} simulation at 30 °C (in red) and 42 °C (in cyan), respectively. Although there is global fold conservation, there are striking local adaptations of secondary elements.

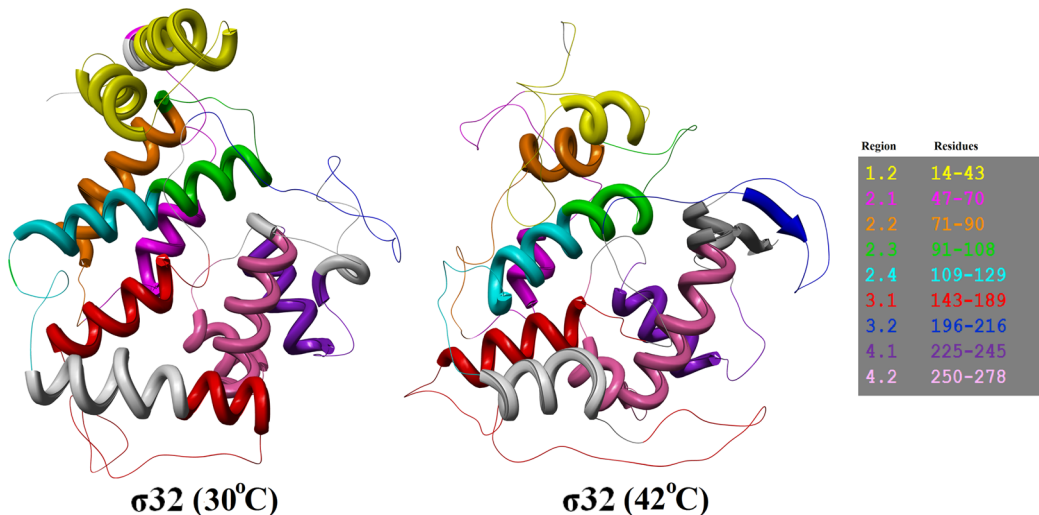


Figure 2. Homology modeled and molecular dynamics refined structure of σ^{32} at 30 and 42 °C. The residues corresponding to respective regions are color coded.¹⁸

(PDB: 1RP3) as was done previously.³⁶ The difference between the current model and the previous model is that the current model is generated with respect to the anti-sigma factor bound complex in the closed state as opposed to the previous one modeled after the open state (PDB: 1IW7).³⁶ This latest model of the whole protein was further refined by extensive molecular dynamics at 30 °C. Root-mean-square deviation from the starting structure was plotted as a function of time (Figure 1). The RMSD value reached a plateau around 230–250 ns, suggesting that the simulation reached an equilibrium state and the calculated value of the RMSD from the initial structure

remained stable at ~ 10 Å for the rest of the simulation time (300 ns, Figure 1). The refined and equilibrated structure (after 300 ns of molecular dynamics simulation) of the current model (Figure 2) shows some interesting features that were not available in the previous model.³⁶ Residues 11–60 of the current model (3D coordinates of the initial 10 residues could not be generated due to lack of a suitable template structure) are largely packed against regions 2.1 and 2.2 (Figures 2 and 4C). A previous study by Raha et al.³⁶ and the current analysis showed significantly high steady-state fluorescence anisotropy values for the single cysteine mutants located within the N

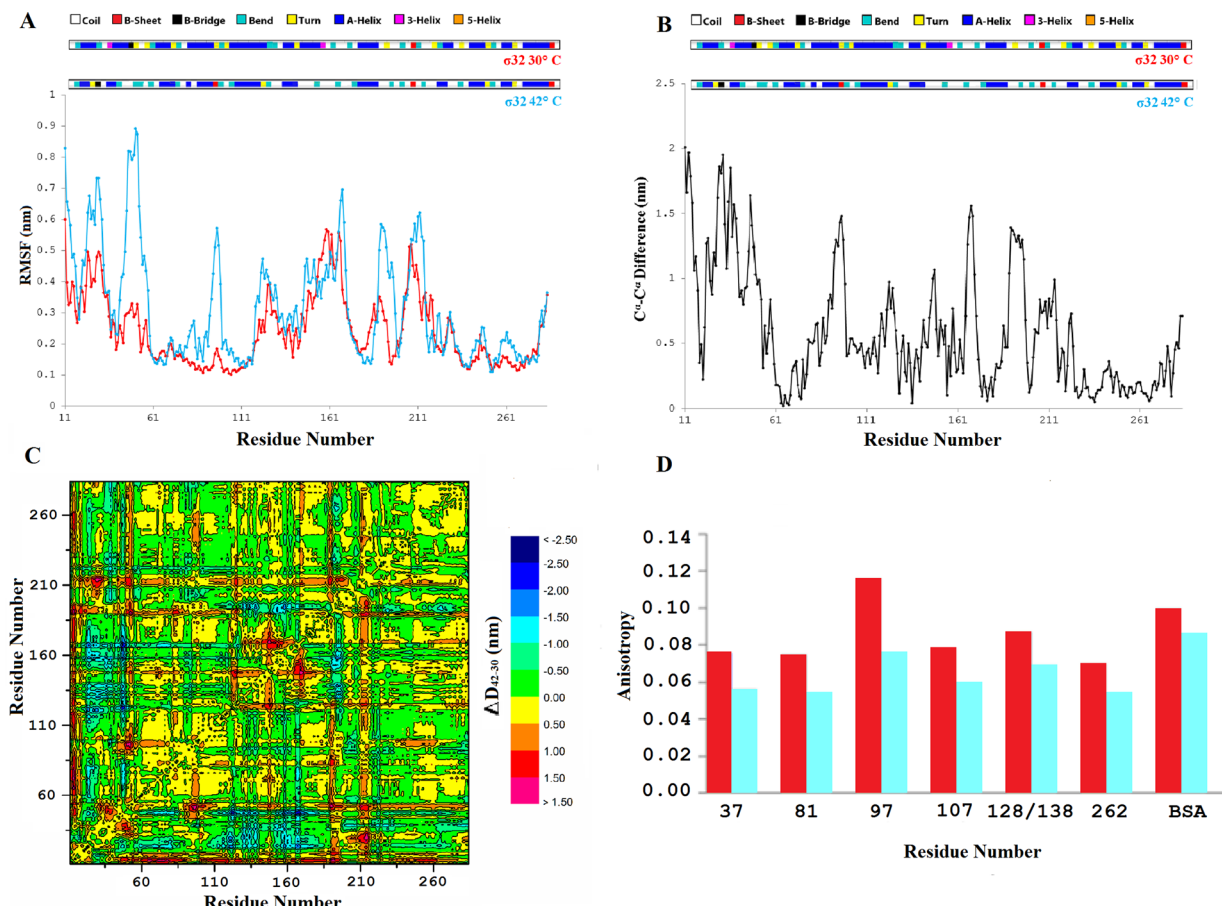


Figure 3. (A) Root-mean-square fluctuation (RMSF) plotted for C^α atoms for simulations of σ³² at temperatures of 30 °C (red) and 42 °C (cyan). The demarcation of secondary structural elements (SSE) present in σ³² at 30 and 42 °C is shown on top. (B) The change in C^α to C^α atomic position between structures saved after 300 ns of simulation at 30 °C and 500 ns of simulation at 42 °C. (C) Heat map representation of deviations in all-atom distance profiles of 300 ns structures obtained for 30 °C and 500 ns structures obtained at 42 °C simulations. ΔD₄₂₋₃₀ is created by subtracting the protein distance contact map of 30 °C from that of 42 °C. (D) Change of fluorescence anisotropy upon temperature up-shift from 30 °C (red) and 42 °C (cyan).

terminal region of the protein (labeled with IAEDANS), suggesting restrictions on freedom of movement. These experimental findings are consistent with our current model of σ³² in which residues 11–60 are not completely free to move. To assess the flapping and lateral movement, i.e., to account for the flexibility, around residues 11–60 and the neighboring regions 2.1–2.3, we monitored the changes in the angle (θ) and dihedral (τ_d) comprising C^α atoms from residues 37–81–107 and 37–81–107–97, respectively. These residues were chosen, as they either encompass or are located close to the probable interacting regions (1.2 and 2.1–2.3) of DnaK and Dnaj. The distance between residues 37 (region 2.1) and 107 (region 2.3) does not change much over the course of the simulation, while regions 2.2 (represented by E81) and 2.3 (V97) get slightly closer (Figure S2 in jp501272n_si_002.pdf in the Supporting Information). Consistent sharp peaks at ~51° (for θ) and about 84° (for τ_d) and also a narrow distribution range were indications that residues 11–60 (mostly belonging to region 1.2) were predominantly confined probably due to their strong packing against residues from region 2.1 to region 2.3 (Figure S3 in jp501272n_si_002.pdf in the Supporting Information). The final structure ($t = 300$ ns) obtained at a simulation temperature of 30 °C has θ and τ_d corresponding to 59 and 94°, respectively, which is close to the

predominant value obtained from the analysis of ensemble structures.

Upon Temperature Up-Shift, σ³² Undergoes a Global Conformational Change. In order to detect any structural change that may occur upon heat shock, molecular dynamics simulation was carried out for 500 ns at 42 °C (Table S1 in jp501272n_si_002.pdf in the Supporting Information) starting with the final structure ($t = 300$ ns) obtained at a simulation temperature of 30 °C. The RMSD values of σ³² (at 42 °C) with respect to the original model structure ($t = 0$ ns) sharply rise and remain much higher than that achieved at 30 °C (Figure 1 and Figure S4 in jp501272n_si_002.pdf in the Supporting Information). Global folds of the two structures (30 and 42 °C) are found to be similar (Figure 2). However, the structures at the local level at 42 °C are substantially different at many places from the corresponding structure at 30 °C (Figures 2 and 3). The overall helix content of the structure at 30 °C is 53% as opposed to 35% for the 42 °C structure (Figure 2 and Figure S5 in jp501272n_si_002.pdf in the Supporting Information). This partial loss of helical structure is consistent with circular dichroism spectra reported in a previous study.¹¹ In the MD simulation, drastic helix melting occurs mostly in the regions 1.2, 2.1, and 2.2 upon temperature up-shift (Figure 2 and Figure S5 in jp501272n_si_001.pdf in the Supporting Information). For example, the helical content of region 1.2

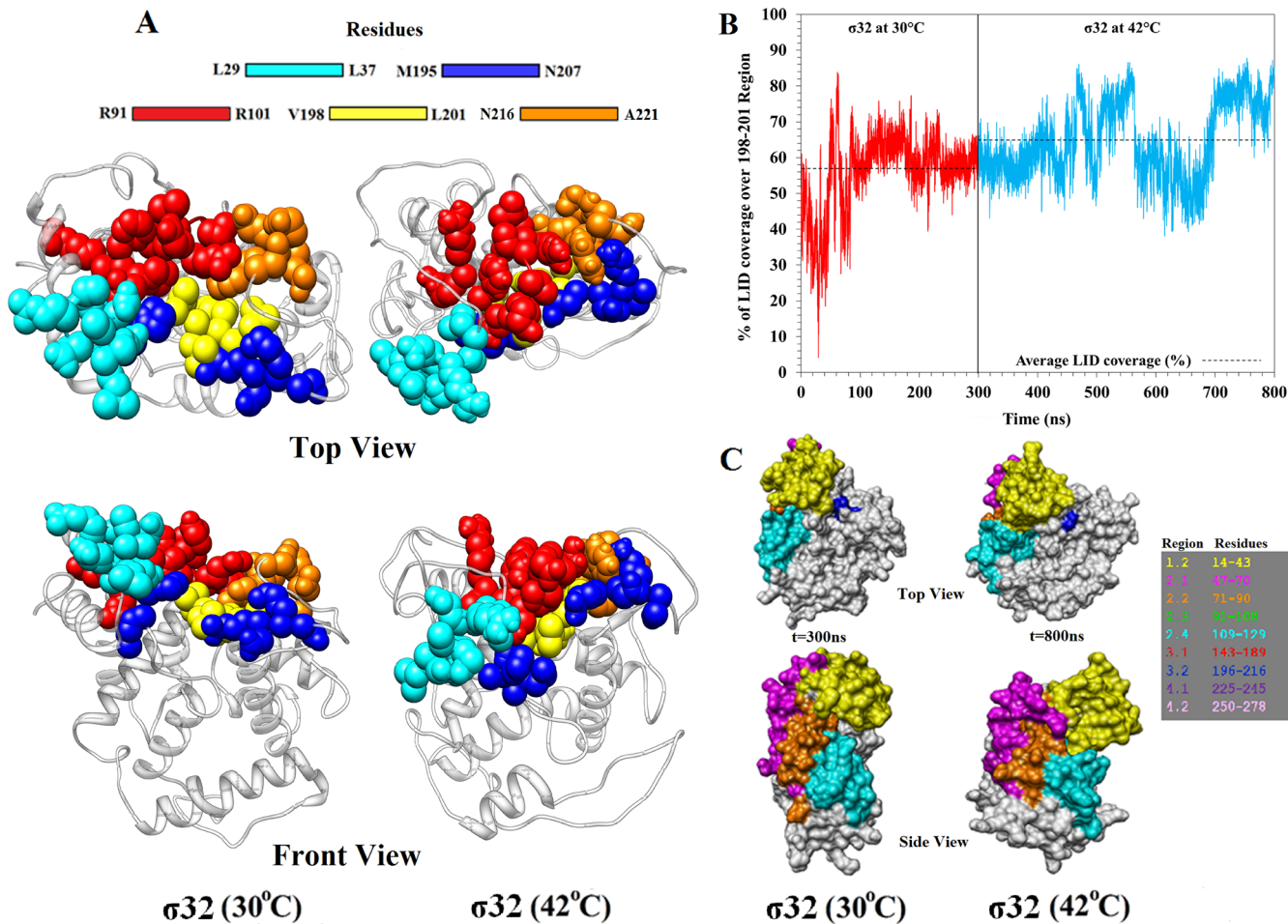


Figure 4. (A) Reduced accessibility of the DNA binding 198-VLYL-201 region upon heat shock. The σ^{32} structures at 30 and 42 °C saved after 300 and 500 ns, respectively, were superimposed and oriented at the same face, and the spacefill representation of the molecule shows the color coded regions corresponding to residues 29–37 (cyan), 91–101 (yellow), 195–207 (blue), 216–221 (orange) and the DnaK binding region (198–201, red). (B) Solvent accessible surface area values of the DnaK binding region (residues 198–201) are plotted against the simulation time. (C) Surface representation of the σ^{32} structures at 30 and 42 °C saved after 300 and 500 ns, showing the color coded regions corresponding to residues 10–46 (yellow), 47–70 (region 2.1, magenta), 71–90 (region 2.2, orange), and 109–129 (region 2.4, sky blue). The DnaK binding region (198–201, blue) at 30 °C (top view, left side panel) has undergone a conformational reorganization at 42 °C (top view, right side panel).

becomes 20% at 42 °C with respect to 70% observed at 30 °C equilibrated structure. Similarly, adjacent 2.1 and 2.2 regions undergo major loss of helical content (31% from 59%) upon temperature elevation. Notwithstanding the helix melting, the N terminal region (residues 11–60) still remains packed against regions 2.1 and 2.2 (Figure 2 and Figure S3 in jp501272n_si_002.pdf in the Supporting Information). The quantification of packing within the 42 °C ensemble structures was also determined by calculating the change in the angle (θ) and dihedral (τ_d) parameters using the C^α atoms from residues 37–81–107 and 37–81–107–97, respectively. The distributions of the angle (θ) and dihedral (τ_d) parameters obtained from the 30 and 42 °C structures are found to be similar apart from a slight shift in dihedral (τ_d) distribution (from +100 to +160) observed for 42 °C structures generating an additional flattened plateau (Figure S3A in jp501272n_si_002.pdf in the Supporting Information).

When the 30 and 42 °C equilibrium structures are compared, large structural rearrangements are seen mostly in three regions of the molecule (Figures 3 and 4). Residues 11–60 undergo significant helix melting (Figure 2) and alteration in structural fluctuations (Figure 3A–C and Figure S6 in

jp501272n_si_002.pdf in the Supporting Information) as pointed out earlier. However, alteration in structural fluctuations and rearrangements are also seen in residues 80–105 and 190–210 (Figure 3 and 4 and Figure S6 in jp501272n_si_002.pdf in the Supporting Information). Equilibrium denaturation studies on σ^{32} showed that the global stability of the protein is not affected and rather a relatively unstable part, possibly the N-terminal domain, gets destabilized at higher temperature.¹¹ This observation is quite well supported by our simulation results, which showed large N-terminal destabilization at 42 °C (Figures 2, 3, and 4 and Figure S6A in jp501272n_si_002.pdf in the Supporting Information). Similarly, structural fluctuations and subsequent destabilization observed around residues 25–60 (Figure 3A and Figure S6 in jp501272n_si_002.pdf in the Supporting Information) might also lead to altered binding with DnaJ, which is reported to bind around residues 31–74 spanning half of the 1.2 and 2.1 regions of σ^{32} .⁷ There are two helices present within residues 31–74 of the σ^{32} structure at 30 °C. However, at 42 °C, the helix spanning residues 31–43 is completely melted while the adjacent helix (residues 75–87) is also melted upon heat shock (Figure S7 in jp501272n_si_002.pdf in the Supporting

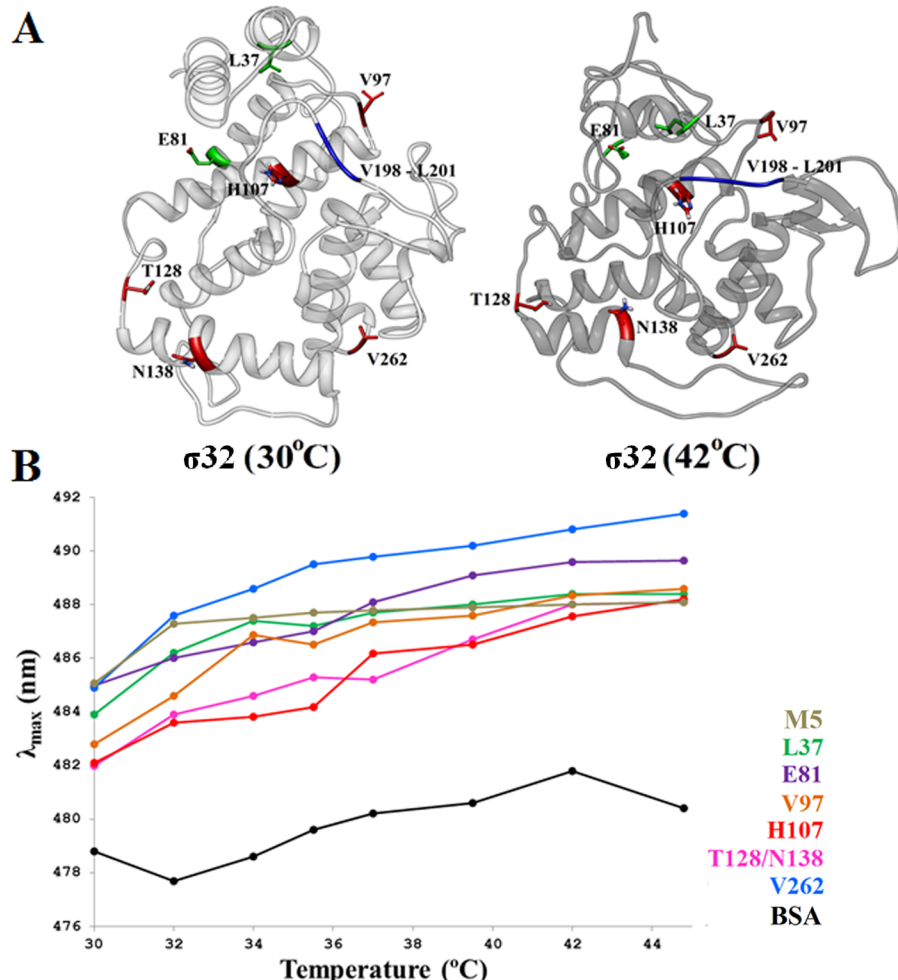


Figure 5. (A) Seven positions in the σ^{32} structure that was mutated to cysteines. Red colored residues represent wavelength maxima shifts of more than 5.5 nm upon shifting of temperature from 30 to 42 °C. Green represents residues cases where the emission maxima shift 4–5 nm, and blue represents residues that shift 3 nm or less. (B) Change in wavelength maxima of the IAEDANS labeled single cysteine mutants of σ^{32} as a function of temperature.

Information). This could lead to altered DnaJ binding which in turn might negatively influence the DnaK binding and subsequent protease degradation by FtsH.^{7,13}

Recent studies have identified residues 198–201 of σ^{32} as the DnaK binding region.⁷ The final structure saved after $t = 500$ ns at 42 °C clearly reflects a higher fluctuation and rearrangement (Figure 3) of residues 190–210, DnaK binding region comprising residues 198–VLYL–201 and residues 216–216 (Figure 4 and Figure S8B–D in jp501272n_si_002.pdf in the Supporting Information). Figure 4 also shows that part of region 2.3 (residues 91–101) and residues 216–221 (Figure 4A and Figure S8B–D in jp501272n_si_002.pdf in the Supporting Information) undergoes melting and conformational change leading to formation of a lid-like structure. This lid sits almost on top of the residues 198–VLYL–201, resulting in reduced accessibility of the DnaK binding regions. In addition, residues 29–37 (Figure 4A) are also found to undergo structural rearrangement, contributing to the reduction of accessibility of the DnaK binding regions. Lid coverage calculation over the DnaK binding region (Figure 4B and Figure S8F,G in jp501272n_si_002.pdf in the Supporting Information) clearly reflects the effect of the structural rearrangement around the DnaK binding region, especially due to 91–101 and 216–221. Both of these regions form a lid-

like structure over the DnaK binding region at 42 °C and result in covering of the DnaK binding site. These structural rearrangements at and around the DnaK binding (198–VLYL–201) region could be associated with loss of DnaK binding upon heat shock. We also observed that the DnaK binding region (198–201) hardly has a counterpart in primary sigma factors, viz., σ^0 , σ^A , σ^{42} , etc., as well as some proteins belonging to the σ^{32} subfamily or σ^{32} homologues (Figures S9 and S10 in jp501272n_si_002.pdf in the Supporting Information). Hence, it could be speculated that the region 198–201 (VLYL) is an insertion and could address specific requirements of σ^{32} which could be associated with temperature up-shift.

The evidence for this temperature dependent global conformational change is also seen in the change of emission maxima values of IAEDANS probes attached to single cysteine residues in going from 30 to 42 °C. σ^{32} has no cysteine residue. Thus, site-directed mutagenesis was used to construct single cysteine mutants at suitable places. The sites chosen for mutagenesis were 37, 81, 97, 107, and 262 (Figure 5A). In addition, a single cysteine mutant was received as a gift from Prof. Bukau which has a cysteine at either residue 128 or 138.³⁷ The V262C mutant was actually a double mutant (L37C, V262C). However, in a previous paper, we have shown that, being a faster-reacting sulphydryl, the 262C becomes labeled

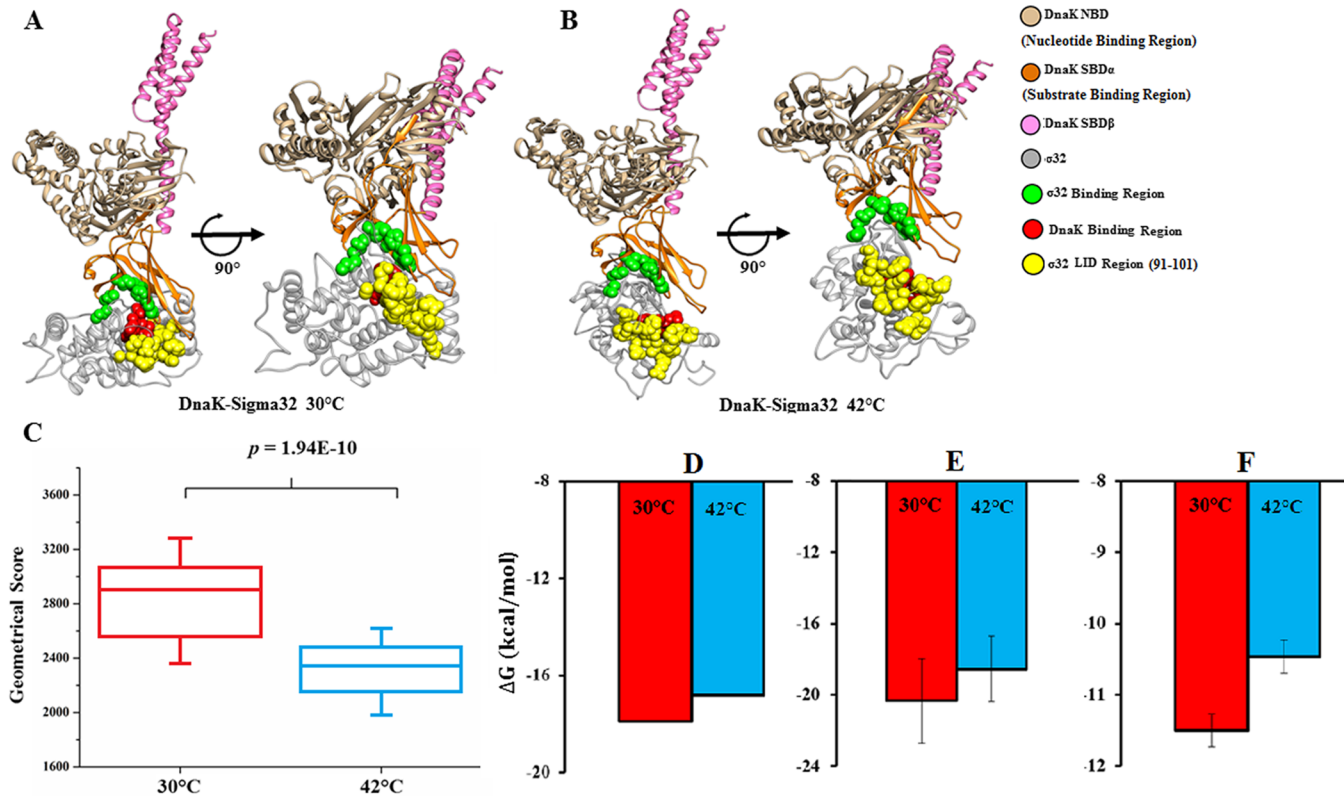


Figure 6. (A) σ^{32} :DnaK complex at 30 °C. (B) σ^{32} :DnaK complex at 42 °C. (C) The geometrical score distribution of the most populated docked cluster obtained from PatchDock. (D) Representation of the lowest theoretical free energy of binding (most favored binding mode) of the complexes at 30 and 42 °C obtained from the 300 and 500 ns time frame, respectively. The free energy values were calculated using the PDBePISA (v1.48) program. DnaK- σ^{32} average represents the mean ΔG value of the highest population cluster. (E) The mean free energy of σ^{32} :DnaK binding obtained from the top solutions of ensemble docking. The ensemble docking was performed with 11 structures from 30 °C (250–300 ns with an interval of 5 ns each) and 42 °C (450–500 ns with an interval of 5 ns each) σ^{32} MD simulation. The top ensemble docking poses from each time frame were selected on the basis of most populated cluster analysis and manual inspection. (F) Depiction of the mean free energy of σ^{32} :DnaK binding obtained from all of the solutions of the most populated cluster of ensemble docking performed on 11 structures from 30 °C (250–300 ns with an interval of 5 ns each) and 42 °C (450–500 ns with an interval of 5 ns each) σ^{32} MD simulation.

under limiting sulphydryl reagent concentrations.¹³ Figure 5B shows the emission maxima changes of IAEDANS labeled single cysteine mutant σ^{32} 's at 30 and 42 °C. Since, in general, some additional solvent exposure may occur due to overall increase in flexibility at higher temperatures, bovine serum albumin (BSA) labeled at its single cysteine residue with AEDANS was used as a control. All the site-specifically labeled σ^{32} proteins show some red shift of emission maxima upon elevation of temperature. Even BSA, which is generally considered a stable protein in this concentration range, shows about 3 nm of emission maxima shift to the red upon increase of temperature. Of the single cysteine mutants, only MSC-AEDANS- σ^{32} shows about 3 nm red shift upon temperature elevation, comparable to the BSA. All other AEDANS- σ^{32} 's show considerably larger red shifts (Figure 5B). Two major patterns may be perceived: First, the change in emission maxima in all of the single cysteine labeled σ^{32} 's, except MSC, is significantly larger than the BSA. Second, there are significant differences between different mutants of σ^{32} . These suggest a global conformational change in which some regions of the protein are more affected than others. Greater emission maxima shifts to the red are shown by three IAEDANS labeled cysteine mutant σ^{32} 's (V97C, H107C, and V262C), all situated in the vicinity of the segment 190–210, which shows a large structural rearrangement between the 30 and 42 °C structures (Figure 5A). In comparison, the other two IAEDANS labeled mutant

σ^{32} 's, L37C and E81C, show a smaller emission maxima shift to the red (~4.5 nm).

Large Increase of Mobility Occurs around the DnaJ and DnaK Binding Sites. Change in dynamics can be an important regulatory component of protein–protein interaction.^{38,39} In order to obtain a better insight into σ^{32} dynamics at 30 and 42 °C, we have analyzed the change in distance among the C^α atoms of the two structures saved at the end of 300 and 500 ns of simulations, respectively. As shown earlier, the C^α to C^α distance plots also depict three dominant regions with distinctly higher fluctuations (Figure 3B). Residues 11–60 at the N-terminus and the 80–105 and 190–210 regions showed high flexibility (Figure 3A and Figure S6A in jpS01272n_si_002.pdf in the Supporting Information). These large amplitudes of flexibility in several segments are consistent with high hydrogen–deuterium exchange rates in much of the σ^{32} structures observed in a previous mass spectrometry study.¹¹ Structural fluctuation and subsequent destabilization observed around N-terminal residues 25–60 might lead to altered binding with DnaJ, which is reported to bind around residues 31–74 of σ^{32} .⁷ This in turn might negatively influence the DnaK binding and subsequent protease degradation by FtsH.¹³ However, the increase in mobility in the DnaK binding region encompassing residues 198–201 is also observed at 42 °C for RUN1 and RUN2 simulations (Table S1 in jpS01272n_si_001.pdf in the Supporting Information). In an

earlier publication, we proposed the region corresponding to 190–205 might adopt an anti-parallel β -hairpin conformation which might become disordered at 42 °C.¹¹ The conformational change seen during molecular dynamic simulation is consistent with the change proposed before.¹¹ In the same study, it was shown that at elevated temperatures this region undergoes enhanced protease cleavage, consistent with the significant structural realignment of this segment, as well as enhanced dynamics upon temperature up-shift observed in the molecular dynamics study (Figures 3 and 4 and Figures S6 and S8 in jp501272n_si_002.pdf in the Supporting Information).

In order to obtain more direct experimental evidence of local enhancement in σ^{32} dynamics, we have measured the change in steady-state anisotropy of previously described IAEDANS labeled single cysteine mutant σ^{32} 's. Figure 3D shows the steady-state anisotropy values. BSA was used as a control. Almost all of the single cysteine labeled protein shows lower anisotropy values than the IAEDANS labeled BSA. However, there are significant differences between the different cysteine mutants at 30 °C. Overall, the differences reported here are consistent with the previously observed values. In the molecular dynamics study, a most interesting increase in flexibility occurs in a small region surrounding residue 97 and in the region encompassing residues 198–201 (Figure 3A and Figure S6A in jp501272n_si_002.pdf in the Supporting Information). In the model, both of the regions are spatially close to each other (around 10 Å). Interestingly, the largest decrease in steady-state anisotropy value upon temperature up-shift among the IAEDANS labeled cysteine mutant proteins was observed for V97C σ^{32} . This is consistent with a large increase of fluctuations in residues 95–100 and 198–201 observed in molecular dynamics study upon temperature up-shift (Figure 3A and Figure S6A in jp501272n_si_002.pdf in the Supporting Information).

Functional Implications of the Conformational Change in σ^{32} . Significant structural changes seen in σ^{32} upon shift to higher temperatures suggest such changes may have functional consequences. Experimentally, weakening of the σ^{32} –DnaK interaction at higher temperatures has been suggested earlier.¹¹ Here, we attempt to investigate the molecular mechanism of disruption of the σ^{32} :DnaK complex at higher temperature via extensive protein–protein docking analysis. Docking of DnaK structure (PDB ID: 4JN4)³⁰ onto the equilibrated structure of σ^{32} was done using the PatchDock program³¹ followed by extensive FireDock³² refinement. Figure 6 shows docking poses of DnaK with respect to the σ^{32} structures at 30 °C (obtained after 300 ns of molecular dynamics simulation) and at 42 °C (obtained after 500 ns of molecular dynamics simulation), respectively. Docking poses were selected on the basis of most populated cluster analysis followed by critical manual inspection satisfying favorable interactions between the interacting motifs of the two proteins.^{7,30} It is evident that the probable binding mode of DnaK is altered and relatively compromised with respect to the σ^{32} structure obtained at 42 °C compared to that obtained at 30 °C. Further, docking scores (geometrical score) and binding energy estimations also suggest (Figure 6C and D) better binding preference to the σ^{32} structure obtained at 30 °C compared to that obtained at 42 °C. We have also performed the ensemble docking simulation again with multiple snapshots. For 30 °C, we selected 11 structures (ranging from 250 to 300 ns with an interval of 5 ns each) and 11 structures at 42 °C (ranging from 450 to 500 ns with an interval of 5 ns each) to

calculate the ensemble average of the free energy of binding between σ^{32} and DnaK protein. The best ensemble docking poses for the multiple snapshots obtained from each time frame were selected on the basis of most populated cluster analysis and manual inspection. The ensemble average obtained after docking also suggests that 30 °C DnaK– σ^{32} binding is stronger compared to 42 °C binding (Figure 6E and F). Similarly, a closer look at the DnaK binding (198–VLYL-201) region within the docked models suggests a much higher presence of DnaK residues within 5 Å distance for the 30 °C σ^{32} structure than that of the 42 °C structure (Figure S11 in jp501272n_si_002.pdf in the Supporting Information).

Another way to validate the structure of the complex obtained by docking is to measure a distance between two fixed points on two proteins. DnaK has a single tryptophan at position 102 which is a suitable partner for a fluorescence resonance energy transfer (FRET) pair. To avoid unambiguous distance measurement between a fixed point in σ^{32} and W102:DnaK, we replaced the single tryptophan in DnaK with 5-OH tryptophan, which shows absorption in wavelengths beyond 300 nm (where tryptophans do not absorb). We have labeled the TN128-138CC mutant of σ^{32} with IAEDANS, which forms a suitable FRET pair with 5-OH tryptophan. The calculated R_0 between the FRET pair is 26.6 Å assuming the κ^2 to be 2/3. Figure 7 shows the comparison of excitation spectra

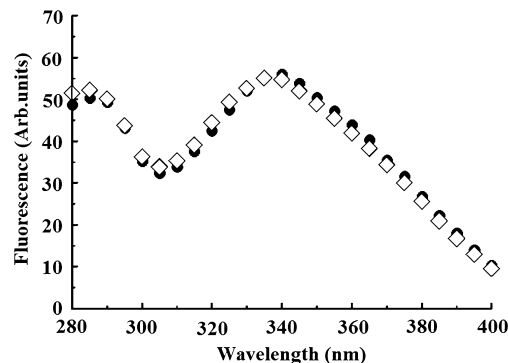


Figure 7. Excitation spectra of IAEDANS labeled σ^{32} /5-OH tryptophan incorporated DnaK complex (●) and IAEDANS labeled σ^{32} (◇) at the same concentrations of proteins and at the same wavelengths. The mixture was allowed to incubate for half an hour, and then the spectra were taken. Emission was at 500 nm, and the band passes were 5 nm each. The measurements were done in 20 mM Hepes pH 7.6, containing 100 mM NaCl, 0.1 mM EDTA, and 25% glycerol.

of IAEDANS labeled σ^{32} (TN128-138CC) alone or in the DnaK complex. There is virtually no difference between the two excitation spectra, suggesting that no energy transfer takes place. This indicates that the distance between the FRET pair is above 53 Å. Figure S12 in jp501272n_si_002.pdf in the Supporting Information shows the $C\alpha$ – $C\alpha$ distances between W102:DnaK and AEDANS- σ^{32} (residues 128 and 138) are 40.2 and 39.5 Å, respectively. Considering the length of the side chain and flexibility of the linkers, the FRET measurements are, thus, not inconsistent with the docked structure.

In the present state-of-the-art, a major conformational change in the docked protein upon binding to its receptor is difficult to capture through a docking protocol. However, if a major conformational change occurs in the protein upon binding to its receptor, it is expected that the fluorescence

quenching pattern of a small molecule quencher toward intrinsic protein fluorescence will be altered. We have thus attempted to measure average collisional quenching parameters for the intrinsic fluorescence of σ^{32} in the bound and free states using acrylamide as the collisional quencher. In order to avoid fluorescence from DnaK, we have labeled the tryptophan by 4-fluorotryptophan which has negligible fluorescence. Figure S13 in jp501272n_si_002.pdf in the Supporting Information shows the acrylamide quenching pattern (Stern–Volmer plot) of the free σ^{32} and in the complex with 4F-Trp-DnaK. After correction for residual DnaK fluorescence, the two plots are remarkably similar, suggesting that no major conformational change occurs in σ^{32} upon complex formation with DnaK.

Further, we have also investigated the impact of structural changes incurred in σ^{32} at higher temperatures on the binding of DnaJ. The 3D model of DnaJ was docked onto the σ^{32} structures, and the binding preferences and interface interactions were observed to be quite altered and compromised with respect to the σ^{32} structure obtained at 42 °C compared to that obtained at 30 °C (Figures S14 and S15 in jp501272n_si_002.pdf in the Supporting Information). On the basis of these observations, we propose two widely varying σ^{32} :DnaK:DnaJ ternary complexes developed using the σ^{32} structure obtained at 30 and 42 °C where the latter is severely compromised in terms of binding energy (Figure S16 in jp501272n_si_002.pdf in the Supporting Information).

CONCLUSION

In this study, through a combination of spectroscopy and molecular dynamics, we have shown that σ^{32} undergoes a global conformational change upon temperature up-shift. Although some structural rearrangement occurs in many segments, two regions appear to be affected the most: residues 11–60 and residues 190–210. The former is responsible for DnaJ binding and further stabilization of the DnaK binding region, whereas the latter residues contain the DnaK binding site (198–201) and residues 192–205 which was previously demonstrated to be an insert having no counterpart in the *E. coli* σ^{70} .¹¹ Residues that have been identified to be important for DnaK binding, 198–201,⁷ form a loop at 30 °C. In the *E. coli* σ^{32} model structure at 30 °C, this loop is solvent exposed but forms the floor of a shallow groove. In the 42 °C structure, the loop gets buried under an adjacent region (residues 91–101 and 216–221) that forms a lid-like structure. Such a rearrangement of the local conformation makes it likely that σ^{32} :DnaK:DnaJ interaction is significantly altered at higher temperatures, as was indicated in a previous study.¹¹ Interestingly, at higher temperature, another part of the protein that shows large deviations from the lower temperature structure lies within residues 11–60. This region is not adjacent to residues 190–210 but is bridged by residues 91–101. The segment 91–101 also shows significant structural changes, suggesting that the effect of structural realignment in segments 190–210 and residues 11–60 may be coupled through this segment. Interestingly, maximum change of hydrogen–deuterium exchange rate is observed in these three segments upon DnaK binding along with that of the extreme C-terminal end.⁷

The combined molecular dynamics and fluorescence spectroscopic study clearly points toward major structural changes in and around residues 11–60 and 190–210 at higher temperatures. The nature of the structural change is such that attenuation of interaction with DnaK/DnaJ is likely at higher temperatures. In fact, our protein–protein docking analyses

suggest that the binding mode of DnaK and DnaJ is indeed altered and relatively compromised with respect to the σ^{32} structure obtained at 42 °C compared to that obtained at 30 °C. If abrogation or attenuation of σ^{32} :DnaK:DnaJ interaction occurs at higher temperatures in the cellular environment, then it would have important implications for the heat-shock response in *E. coli*. Previously, two other mechanisms of σ^{32} stabilization at higher temperatures have been proposed: (1) enhanced translation of σ^{32} mRNA at elevated temperatures⁴⁰ and (2) titration away of DnaK from the σ^{32} :DnaK:DnaJ complex by increased concentrations of unfolded proteins at higher temperatures.² Although both of these mechanisms may exist, they are likely to have slower kinetics, whereas, if the σ^{32} adopts a conformational change with respect to higher temperature, the initiation of heat-shock response is likely to be faster. In conclusion, we have observed a temperature dependent conformational change in σ^{32} structure at elevated temperatures which alters the accessibility of the DnaK binding site and changes the secondary structural arrangement near the DnaJ binding site, leading to compromised σ^{32} :DnaK:DnaJ complex formation and/or probable disruption of the complex.

ASSOCIATED CONTENT

Supporting Information

Detailed information regarding the fluorescence spectroscopic protocols and computational analysis performed in this study can be found in jp501272n_si_001.pdf. Background experiments with figures supporting the conclusions drawn in the manuscript can be found in jp501272n_si_002.pdf. This material is available free of charge via the Internet at <http://pubs.acs.org>.

AUTHOR INFORMATION

Author Contributions

[†]A.C. and S.M. contributed equally.

Notes

The authors declare no competing financial interest.

ACKNOWLEDGMENTS

We would like to acknowledge Dr. Tuhin Kumar Pal for his initial effort in building the σ^{32} model structure.

REFERENCES

- (1) Morimoto, R. I. The Heat Shock Response: Systems Biology of Proteotoxic Stress in Aging and Disease. *Cold Spring Harbor Symp. Quant. Biol.* **2011**, *76*, 91–99.
- (2) Arsene, F.; Tomoyasu, T.; Bukau, B. The Heat Shock Response of Escherichia coli. *Int. J. Food Microbiol.* **2000**, *55* (1–3), 3–9.
- (3) Helmann, J. D.; Chamberlin, M. J. Structure and Function of Bacterial Sigma Factors. *Annu. Rev. Biochem.* **1988**, *57*, 839–872.
- (4) Helmann, J. D. Anti-Sigma Factors. *Curr. Opin Microbiol.* **1999**, *2* (2), 135–141.
- (5) Helmann, J. D. The Extracytoplasmic Function (ECF) Sigma Factors. *Adv. Microb. Physiol.* **2002**, *46*, 47–110.
- (6) Gamer, J.; Bujard, H.; Bukau, B. Physical Interaction Between Heat Shock Proteins DnaK, DnaJ, and GrpE and the Bacterial Heat Shock Transcription Factor Sigma 32. *Cell* **1992**, *69* (5), 833–842.
- (7) Rodriguez, F.; Arsene-Pioletz, F.; Rist, W.; Rudiger, S.; Schneider-Mergener, J.; Mayer, M. P.; Bukau, B. Molecular Basis for Regulation of the Heat Shock Transcription Factor Sigma32 by the DnaK and DnaJ Chaperones. *Mol. Cell* **2008**, *32* (3), 347–358.
- (8) Straus, D. B.; Walter, W. A.; Gross, C. A. The Heat Shock Response of *E. coli* is Regulated by Changes in the Concentration of Sigma 32. *Nature* **1987**, *329* (6137), 348–351.

- (9) Guisbert, E.; Yura, T.; Rhodius, V. A.; Gross, C. A. Convergence of Molecular, Modeling, and Systems Approaches for an Understanding of the Escherichia coli Heat Shock Response. *Microbiol. Mol. Biol. Rev.* **2008**, *72* (3), 545–554.
- (10) Bukau, B. Regulation of the Escherichia coli Heat-Shock Response. *Mol. Microbiol.* **1993**, *9* (4), 671–680.
- (11) Chattopadhyay, R.; Roy, S. DnaK-Sigma 32 Interaction is Temperature-Dependent. Implication for the Mechanism of Heat Shock Response. *J. Biol. Chem.* **2002**, *277* (37), 33641–33647.
- (12) Rist, W.; Jorgensen, T. J.; Roepstorff, P.; Bukau, B.; Mayer, M. P. Mapping Temperature-Induced Conformational Changes in the Escherichia coli Heat Shock Transcription Factor Sigma 32 by Amide Hydrogen Exchange. *J. Biol. Chem.* **2003**, *278* (51), 51415–51421.
- (13) Horikoshi, M.; Yura, T.; Tsuchimoto, S.; Fukumori, Y.; Kanemori, M. Conserved Region 2.1 of Escherichia coli Heat Shock Transcription Factor Sigma32 is Required for Modulating Both Metabolic Stability and Transcriptional Activity. *J. Bacteriol.* **2004**, *186* (22), 7474–7480.
- (14) The Universal Protein Resource (UniProt) in 2010. *Nucleic Acids Res.* **2010**, *38* (Database issue), D142–148.
- (15) Soding, J.; Biegert, A.; Lupas, A. N. The HHpred Interactive Server for Protein Homology Detection and Structure Prediction. *Nucleic Acids Res.* **2005**, *33* (Web Server issue), W244–248.
- (16) Kelley, L. A.; Sternberg, M. J. Protein Structure Prediction on the Web: A Case Study Using the Phyre Server. *Nat. Protoc.* **2009**, *4* (3), 363–371.
- (17) Jones, D. T. Protein Secondary Structure Prediction Based on Position-Specific Scoring Matrices. *J. Mol. Biol.* **1999**, *292* (2), 195–202.
- (18) Sali, A.; Blundell, T. L. Comparative Protein Modelling by Satisfaction of Spatial Restraints. *J. Mol. Biol.* **1993**, *234* (3), 779–815.
- (19) Huang, K.; Flanagan, J. M.; Prestegard, J. H. The Influence of C-terminal Extension on the Structure of the “J-domain” in E. coli DnaJ. *Protein Sci.* **1999**, *8* (1), 203–214.
- (20) Barends, T. R.; Brosi, R. W.; Steinmetz, A.; Scherer, A.; Hartmann, E.; Eschenbach, J.; Lorenz, T.; Seidel, R.; Shoeman, R. L.; Zimmermann, S.; et al. Combining Crystallography and EPR: Crystal and Solution Structures of the Multidomain Chaperone DnaJ. *Acta Crystallogr., Sect. D: Biol. Crystallogr.* **2013**, *69* (Pt 8), 1540–1552.
- (21) Kiefer, F.; Arnold, K.; Kunzli, M.; Bordoli, L.; Schwede, T. The SWISS-MODEL Repository and Associated Resources. *Nucleic Acids Res.* **2009**, *37* (Database issue), D387–392.
- (22) Li, J.; Qian, X.; Sha, B. The Crystal Structure of the Yeast Hsp40 Ydj1 Complexed with its Peptide Substrate. *Structure* **2003**, *11* (12), 1475–1483.
- (23) Martinez-Yamout, M.; Legge, G. B.; Zhang, O.; Wright, P. E.; Dyson, H. J. Solution Structure of the Cysteine-Rich Domain of the Escherichia coli Chaperone Protein DnaJ. *J. Mol. Biol.* **2000**, *300* (4), 805–818.
- (24) Lindahl, E.; Azuara, C.; Koehl, P.; Delarue, M. NOMAD-Ref: Visualization, Deformation and Refinement of Macromolecular Structures Based on All-Atom Normal Mode Analysis. *Nucleic Acids Res.* **2006**, *34* (Web Server issue), WS2–56.
- (25) Van Der Spoel, D.; Lindahl, E.; Hess, B.; Groenhof, G.; Mark, A. E.; Berendsen, H. J. GROMACS: Fast, Flexible, and Free. *J. Comput. Chem.* **2005**, *26* (16), 1701–1718.
- (26) Oostenbrink, C.; Villa, A.; Mark, A. E.; van Gunsteren, W. F. A Biomolecular Force Field Based on the Free Enthalpy of Hydration and Solvation: The GROMOS Force-Field Parameter Sets 53A5 and 53A6. *J. Comput. Chem.* **2004**, *25* (13), 1656–1676.
- (27) Konagurthu, A. S.; Reboul, C. F.; Schmidberger, J. W.; Irving, J. A.; Lesk, A. M.; Stuckey, P. J.; Whisstock, J. C.; Buckle, A. M. MUSTANG-MR Structural Sieving Server: Applications in Protein Structural Analysis and Crystallography. *PLoS One* **2010**, *5* (4), e10048.
- (28) Humphrey, W.; Dalke, A.; Schulten, K. VMD: Visual Molecular Dynamics. *J. Mol. Graphics* **1996**, *14* (1), 33–38 27–28..
- (29) Pettersen, E. F.; Goddard, T. D.; Huang, C. C.; Couch, G. S.; Greenblatt, D. M.; Meng, E. C.; Ferrin, T. E. UCSF Chimera—A
- Visualization System for Exploratory Research and Analysis. *J. Comput. Chem.* **2004**, *25* (13), 1605–1612.
- (30) Qi, R.; Sarbeng, E. B.; Liu, Q.; Le, K. Q.; Xu, X.; Xu, H.; Yang, J.; Wong, J. L.; Vorvis, C.; Hendrickson, W. A.; et al. Allosteric Opening of the Polypeptide-Binding Site When an Hsp70 Binds ATP. *Nat. Struct Mol. Biol.* **2013**, *20* (7), 900–907.
- (31) Schneidman-Duhovny, D.; Inbar, Y.; Nussinov, R.; Wolfson, H. J. PatchDock and SymmDock: Servers for Rigid and Symmetric Docking. *Nucleic Acids Res.* **2005**, *33* (WebServer issue), W363–367.
- (32) Andrusier, N.; Nussinov, R.; Wolfson, H. J. FireDock: Fast Interaction Refinement in Molecular Docking. *Proteins* **2007**, *69* (1), 139–159.
- (33) Krissinel, E.; Henrick, K. Inference of Macromolecular Assemblies from Crystalline State. *J. Mol. Biol.* **2007**, *372* (3), 774–797.
- (34) Sorenson, M. K.; Ray, S. S.; Darst, S. A. Crystal Structure of the Flagellar Sigma/Anti-Sigma Complex Sigma(28)/FlgM Reveals an Intact Sigma Factor in an Inactive Conformation. *Mol. Cell* **2004**, *14* (1), 127–138.
- (35) Campbell, E. A.; Masuda, S.; Sun, J. L.; Muzzin, O.; Olson, C. A.; Wang, S.; Darst, S. A. Crystal Structure of the Bacillus stearothermophilus Anti-Sigma Factor SpoIIAB with the Sporulation Sigma Factor SigmaF. *Cell* **2002**, *108* (6), 795–807.
- (36) Raha, P.; Chattopadhyay, S.; Mukherjee, S.; Chattopadhyay, R.; Roy, K.; Roy, S. Alternative Sigma Factors in the Free State are Equilibrium Mixtures of Open and Compact Conformations. *Biochemistry* **2010**, *49* (45), 9809–9819.
- (37) Arsene, F.; Tomoyasu, T.; Mogk, A.; Schirra, C.; Schulze-Specking, A.; Bukau, B. Role of Region C in Regulation of the Heat Shock Gene-Specific Sigma Factor of Escherichia coli, Sigma32. *J. Bacteriol.* **1999**, *181* (11), 3552–3561.
- (38) Tzeng, S. R.; Kalodimos, C. G. Dynamic Activation of an Allosteric Regulatory Protein. *Nature* **2009**, *462* (7271), 368–372.
- (39) Popovych, N.; Sun, S.; Ebright, R. H.; Kalodimos, C. G. Dynamically Driven Protein Allostery. *Nat. Struct Mol. Biol.* **2006**, *13* (9), 831–838.
- (40) Nagai, H.; Yuzawa, H.; Yura, T. Interplay of Two Cis-Acting mRNA Regions in Translational Control of Sigma 32 Synthesis During the Heat Shock Response of Escherichia coli. *Proc. Natl. Acad. Sci. U.S.A.* **1991**, *88* (23), 10515–10519.